ACS Sustainable Chemistry & Engineering

Research Article

pubs.acs.org/journal/ascecg

Dissolved Phosphorus Speciation of Flash Carbonization, Slow Pyrolysis, and Fast Pyrolysis Biochars

Minori Uchimiya,*[,†] Syuntaro Hiradate,[‡] and Michael Jerry Antal, Jr.[§]

[†]USDA-ARS Southern Regional Research Center, 1100 Robert E. Lee Boulevard, New Orleans, Louisiana 70124, United States

[‡]National Institute for Agro-Environmental Sciences, 3-1-3 Kan-nondai, Tsukuba, Ibaraki 305-8604, Japan

[§]Hawaii Natural Energy Institute, School of Ocean and Earth Science and Technology, University of Hawaii at Manoa, Honolulu, Hawaii 96822, United States

Supporting Information

ABSTRACT: Pyrolysis of waste biomass is a promising technology to produce sterile and renewable organic phosphorus fertilizers. Systematic studies are necessary to understand how different pyrolysis platforms influence the chemical speciation of dissolved (bioavailable) phosphorus. This study employed solution-phase ^{31}P NMR analyses on slow pyrolysis, fast pyrolysis, and flash carbonization charcoals. Dissolved P speciation of ash-rich (15−62 wt %) biochars produced from manures, sewage sludge, and corn stover were compared with low ash (2−5 wt %) pecan shell biochars. Each biochar was sequentially extracted to investigate the strongly complexed (by NaOH−EDTA; 250 mM NaOH+5 mM EDTA for 16 h) and acid-extractable (by acidic oxalate; 200 mM oxalate at pH 3.5 for 4 h) P fractions. In NaOH−EDTA extracts, P concentration correlated ($p < 0.0005$) with Zn ($r = 0.89$), Mn ($r = 0.90$), and Mg ($r = 0.98$) concentrations. A strong correlation between orthophosphate and Mg ($r = 0.98$, $p < 0.0005$; $n = 13$) indicated the presence of Mg orthophosphate (and struvite or whitlockite) in all biochars. Only in acidic oxalate extracts, P concentration correlated ($p < 0.0005$) with Al ($r = 0.87$) and Fe ($r = 0.92$) concentrations. Pyrophosphate ($P_2O_7^{4-}$) persisted (23−52% of total P in NaOH−EDTA extracts) in low-ash pecan shell 300−700 °C slow pyrolysis biochars. In contrast, ash-rich biochars were primarily (≥90%) composed of inorganic orthophosphate (PO_4^{3-}), except 350 °C slow pyrolysis swine manure biochar (26% pyrophosphate) and sewage sludge-derived flash carbonization charcoal (14% pyrophosphate). Solid-state ^{13}C cross-polarization and magic angle spinning NMR analyses of bulk aromaticity indicated partially carbonized (aliphatic) nature of 350 °C swine manure biochar. Surface functional groups of swine manure and sewage sludge biochars could stabilize pyrophosphate by (i) utilizing bridging cations (Al^{3+}, Fe^{3+}, and Mg^{2+}) to form stable six-membered ring complexes, and (ii) direct hydrogen bonding.

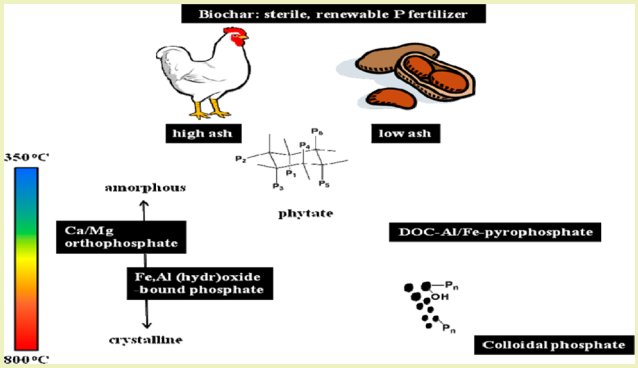

KEYWORDS: *Soil amendment, Remediation, Waste management, Bioenergy, Nutrient*

INTRODUCTION

Mined phosphate rock is the primary chemical phosphorus fertilizer worldwide.[1] It is widely accepted that the world's reserve of rock phosphate will become depleted in the next several decades.[2] Although biochar continues to receive interests as a sterile, renewable phosphorus fertilizer, limited studies are available to understand how different pyrolysis conditions influence the dissolved (bioavailable) phosphorus speciation. Our previous study compared biochars produced by the slow pyrolysis of plant (cottonseed hull) and manure (broiler litter) feedstocks at 350, 500, 650, and 800 °C.[3] For plant biochars, NaOH−EDTA (250 mM NaOH+5 mM EDTA for 16 h)-extractable P was greater than oxalate (200 mM oxalate at pH 3.5 for 4 h), and the opposite trend was observed for manure biochars.[3] Solution-phase ^{31}P NMR analysis of NaOH−EDTA extracts showed the conversion of phytate to inorganic P by pyrolysis of manure and plant feedstocks at 350 °C. Inorganic orthophosphate (PO_4^{3-}) became the sole species of ≥500 °C manure biochars, whereas pyrophosphate ($P_2O_7^{4-}$) persisted in plant biochars up to 650 °C. These observations suggested the predominance of mixed phase (amorphous and crystalline) calcium phosphate in ≥650 °C manure biochars.[3] Pyrophosphate was likely stabilized in 350−500 °C plant biochars by forming complexes with the organic carbon fraction of biochar. Both amorphous minerals[4] and organic carbon (to form organic carbon−metal−phosphate complexes)[5,6] are known to control P speciation in Andosol and other fire-impacted soils.

Received: April 21, 2015
Published: June 2, 2015

DOI: 10.1021/acssuschemeng.5b00336
ACS Sustainable Chem. Eng. 2015, 3, 1642−1649

The present study will focus on three different pyrolysis platforms (slow pyrolysis, fast pyrolysis, and flash carbonization) that influenced the aromaticity of dissolved organic carbon (DOC) extracted from biochar.[7] We emphasize that the reported feedstock and pyrolysis conditions will influence, but do not determine, the properties of biochar.[8] Importantly, the thermocouple used to measure heat treatment temperature (HTT), or peak temperature, does not measure the actual temperature of the biomass particles during pyrolysis. For example, fast pyrolysis reactors designed to maximize oil yield (and minimize charcoal formation) employ high heating rates (>1000 °C s^{-1}). As a result, the pyrolysis reactions are endothermic, and there is a large temperature difference (i.e., "thermal lag") between the solid product and its surrounding gaseous environment. Consequently, the temperature of biomass particles undergoing pyrolysis can be hundreds of degrees Celsius below its environment.[9,10] In contrast, pyrolysis reactor designed to maximize the charcoal yield will evoke exothermic pyrolysis reactions in the biomass.[11] As a result, the temperature of charcoal can be much higher than its HTT.[11] In summary, a thermocouple placed in the gaseous environment of a biomass particle undergoing pyrolysis does not measure the temperature at which pyrolysis is actually occurring; the thermocouple merely measures its own temperature, and this fact is well-known in the field of fuel chemistry.

The objective of the present study was two-hold: (i) investigate the influence of three different pyrolysis platforms (flash carbonization,[11] slow pyrolysis, and fast[12] pyrolysis) on P speciation in NaOH−EDTA extracts, and (ii) identify the remaining soluble P species by utilizing the sequential extraction, i.e., basic EDTA followed by acidic oxalate. This study will focus on feedstocks containing significant amounts of ash, where bioavailable P is expected to exist: sewage sludge, corn stover, and manure. Solution-phase ^{31}P NMR analysis of the sequential extracts will allow us to identify (i) P species bound to minerals, e.g., Fe and Al (hydr)oxides, and strongly complexed by organic carbon fraction of biochar in the NaOH−EDTA extract, and (ii) remaining phases sensitive to acid dissolution, e.g., calcium phosphate, in the oxalate extract.

MATERIALS AND METHODS

Distilled, deionized water (DDW) with a resistivity of 18 MΩ cm (Millipore, Milford, MA) was used for all procedures. Unless otherwise noted, all chemical reagents were obtained from Sigma-Aldrich (Milwaukee, WI) with the highest purity available.

Slow Pyrolysis. Pecan shells (PS25) were obtained from sheller and were ground (SM 2000 cutting mill, Retsch Gmbh, Haan, Germany) and sieved to <2 mm.[13] Feedstocks were pyrolyzed at 300, 500, and 700 °C under 1600 mL min^{-1} N_2 flow rate for 4 h using a laboratory scale box furnace (22 L void volume) with a retort (Lindberg, Type 51662-HR, Watertown, WI). Biochar products were allowed to cool to room temperature overnight under N_2 atmosphere. Biochars are hereby denoted by the feedstock abbreviation and pyrolysis temperature, e.g., pecan shell feedstock (PS25) and biochars produced at 300 (PS300) and 500 °C (PS500). Feedlot (FL) and swine (SW) manures and corresponding 350 and 700 °C biochars were received from USDA-ARS Florence, SC employing a similar slow pyrolysis unit with ≈10 °C min^{-1} heating rate and 2 h hold time at the peak temperature.[14] Feedlot manure (FL) was obtained from a commercial deep-bedded (corn stalks were rebedded every week) facility, and contained 77.9 ± 0.5 wt % moisture.[14] Separated swine solids (SW, 78.5 ± 0.5 wt % moisture) were obtained from a commercial swine operation utilizing polyacrylamide (PAM) and phosphate precipitation sludge[15] to treat 1 week-old flushed swine manure.[14]

Flash Carbonization. The University of Hawaii's patented Flash Carbonization process uses starved-air combustion at elevated pressure for carbonization.[16] Corn stover (corn) and sewage sludge (sewage) Flash Carbonization charcoals[16] were produced at the University of Hawaii Flash Carbonization pilot plant facility. The temperature and reaction time employed to produce each charcoal varied according to the feedstock properties, its moisture content, and the desired quality (i.e., fixed-carbon content) of the charcoal. All Flash Carbonization charcoals were ground and sieved to <2 mm.

Fast Pyrolysis. Fast pyrolysis involves rapid heating (>1000 °C s^{-1}) and short residence time to maximize the yield of liquid product (bio-oil).[17] Fast pyrolysis biochar (FP) was produced at 500 °C from mixed sawdust by Dynamotive Energy Systems (Vancouver, BC, Canada) using an industrial-scale bubbling fluidized bed reactor designed to yield 60−75 wt % bio-oil, 15−20 wt % biochar, and 10−20 wt % syngas.[12] The FP was a fine powder, and was used as received in a sealed drum.

Solution-Phase ^{31}P NMR Analysis of Basic EDTA and Acidic Oxalate Sequential Extracts. Solution-phase ^{31}P NMR samples were obtained by sequential extraction steps (each denoted by the abbreviation in parentheses): basic EDTA (NaOH−EDTA) followed by acidic ammonium oxalate (oxalate). For each feedstock and biochar, 5 g of sample was shaken in 100 mL of 250 mM NaOH+5 mM EDTA for 16 h, and was then centrifuged at 900*g* for 30 min and vacuum filtered through Whatman no. 42 (2.5 μm) filter paper.[18] Subsequently, retained solids were shaken in 100 mL of 0.2 M ammonium oxalate (pH 3.5) for 4 h in the dark, and then centrifuged and vacuum filtered through Whatman no. 42 filter paper. Visible calcium oxalate precipitates formed during the acidic ammonium oxalate extraction. Aliquots from NaOH−EDTA and oxalate extractions were acidified to 4 vol % nitric acid (trace metal grade) for the determination of dissolved P, K, Ca, Mg, Al, Fe, Mn, and Na concentrations using inductively coupled plasma atomic emission spectrometry (ICP-AES; Profile Plus, Teledyne/Leeman Labs, Hudson, NH). Blanks, blank spikes, and matrix spikes were included for the quality assurance and control for the ICP-AES analysis.[19] Electric conductivity (EC), pH, and total organic carbon (TOC) content of 16 h cold (25 °C)[7] and hot (80 °C)[7] water extracts (biochar:DDW (w/w) = 1:10)[7] and proximate analysis[7,13,14,20] results were obtained from the literature.

To concentrate samples for the ^{31}P NMR analysis,[18] filtered NaOH−EDTA and oxalate extracts were freeze-dried. The NMR sample was obtained by dissolving 100 mg of freeze-dried sample in 0.6 mL of 1 M NaOH in 10% D_2O. The ^{31}P NMR spectra were obtained using Alpha 600 FT NMR spectrometer (JEOL, Tokyo) with a 5 mm probe. Spectra were recorded at 242.85 MHz using a pulse width of 10.00 μs (90°), an acquisition time of 0.4522 s, and broadband proton decoupling at 30 °C. The pulse delay time of 2 s was employed.[21] Each spectrum was scanned 30 000 times and a broadening factor of 5.00 Hz was used in the Fourier transform procedure. Chemical shifts (ppm) were determined with respect to 85% H_3PO_4 solution (0 ppm). The total signal intensity and the fraction contributed by each P compound were calculated by integration of the spectral signals using Alice 2 for Windows version 5.1.1 (JEOL, Tokyo).

Solid-State ^{13}C NMR. Solid-state ^{13}C cross-polarization and magic angle spinning (CPMAS) NMR was employed to investigate the influence of pyrolysis techniques on the bulk aromaticity and other structural components of organic carbon in fast pyrolysis, flash carbonization (sewage and corn), and slow pyrolysis (FL350, FL700, SW350, and SW700) biochars.[22] The ^{13}C signals of finely ground powder in KEL-F spinning tube (6 mm diameter, JEOL, Tokyo, Japan) were recorded at 75.45 MHz with a magic angle spinning of 6 kHz, 1 ms of contact time, and 3 s of pulse interval with 100 Hz broadening factor for the Fourier transform. The chemical shifts were interpreted with respect to tetramethylsilane and adamantane external reference (29.50 ppm). Resulting ^{13}C NMR spectra were interpreted on the basis of chemical shift regions (in ppm): aliphatic C (0−45), O/N alkyl C (45−110), aromatic C (110−160), and carbonyl C (160−190).[22]

DOI: 10.1021/acssuschemeng.5b00336
ACS Sustainable Chem. Eng. 2015, 3, 1642−1649

Table 1. Dissolved Phosphorus Concentrations in the Sequential (NaOH−EDTA then oxalate) and Water Extracts of Corn Stover (Corn) and Sewage Sludge (Sewage) Flash Carbonization Charcoals; Sawdust-Derived Fast Pyrolysis Biochar (FP); and Feedlot (FL), Swine (BL), and Pecan Shell (PS) Slow Pyrolysis (300-700 °C) Biochars[a]

					proximate analysis (wt $\%_{dry}$)[d]			P in mg kg^{-1}		
biochar	pH	EC (mS cm^{-1})	TOC ppm of C	extraction method	ash	fixed C	VM	EDTA	oxalate	water
corn	7.5	1.9	1516	cold water[b]	16.6(1.5)	51.4(2.7)	32.0(2.5)	1302	405	3[b]
sewage	5.3	17.9	22	cold water[b]	61.6(6.7)	15.5(2.0)	22.9(7.8)	16718	7719	21[b]
FP	6.2	0.5	282	cold water[b]	5.6(0.2)	62.7(0.3)	31.6(0.4)	120	27	N/A
FL25	6.9	5.2	3447	cold water[b]	15.4(0.2)	7.9(0.6)	76.7(0.5)	6995	514	3070[e]
FL350	7.7	6.6	619	cold water[b]	28.7(0.7)	23.5(3.4)	47.9(2.8)	11853	587	460[e]
FL700	10.5	8.7	59	cold water[b]	44.0(0.0)	36.3(1.6)	19.8(1.6)	5349	N/A	180[e]
SW25	7.0	3.5	1826	cold water[b]	20.9(0.4)	5.6(0.1)	73.6(0.3)	20438	3207	11000[e]
SW350	7.7	2.1	106	cold water[b]	32.5(0.9)	17.7(1.2)	49.8(0.6)	24120	5160	390[e]
SW700	8.7	1.9	5	cold water[b]	52.9(0.5)	33.8(0.5)	13.4(0.3)	22886	8634	60[e]
PS25	4.3	0.0	852	hot water[b]	1.5(0.2)	26.5(2.3)	72.1(2.1)	141	21	N/A
PS300	N/A	N/A	N/A		1.9(0.0)	41.9(0.5)	56.2(0.5)	224	17	N/A
PS500	7.7	0.6	146	hot water[c]	3.8(0.1)	76.7(0.1)	19.5(0.1)	81	12	N/A
PS700	9.5	0.7	18	hot water[c]	4.5(0.0)	86.9(0.1)	8.7(0.2)	50	18	N/A

[a]Proximate analysis results, pH, electric conductivity (EC), and total organic carbon (TOC) are the literature values.[7,49] [b]Cold (25 °C)[7] water extractions for 16 h at 100 g L^{-1}. [c]Hot (80 °C)[49] water extractions for 16 h at 100 g L^{-1}. [d]Literature values for mean and s.d. (in parentheses) of 3 replicate.[7,13,14,20] [e]Water-soluble P.[14]

RESULTS AND DISCUSSION

Dissolved Phosphorus Contents of Flash Carbonization and Slow/Fast Pyrolysis Biochars. Table 1 presents dissolved P concentrations (in mg kg^{-1} biochar) for flash carbonization charcoals prepared from corn stover (corn) and sewage sludge (sewage); sawdust-derived fast pyrolysis biochar (FP); and slow pyrolysis 300−700 °C biochars produced from swine (SW) and feedlot (FL) manures and pecan shell (PS). Extracts were obtained sequentially in NaOH−EDTA (250 mM NaOH+5 mM EDTA for 16 h) and then oxalate (200 mM oxalate at pH 3.5 for 4 h). Table 1 indicates high ash contents (15−62 wt %) of all biochars except FP and 300−700 °C pecan shell biochars (<6 wt %). Ash-rich (manure and sewage sludge) biochars contained orders of magnitude higher NaOH−EDTA-extractable P than pecan shell biochars. The NaOH−EDTA-extractable P increased at 300−350 °C, and decreased at higher temperatures for both plant and manure slow pyrolysis biochars. Water-soluble P concentration often decreases at higher pyrolysis temperatures[14] by the formation of stable minerals[23] and other tightly bound P species. Typically, total P content progressively increases as a function of temperature, and are several orders of magnitude higher in ash-rich manure and sewage sludge biochars than plant biochars.[3,23] Total P is determined by digestion methods aimed to maximize P recovery by ensuring oxidation of recalcitrant C,[24] while minimizing the volatilization loss of P occurring near 760 °C.[25] Depending on the digestion method, recovery of total phosphorus from biochars can vary by orders of magnitude.[24]

Inorganic P in manure is primarily associated with >0.45 μm particulate solids of Ca and Mg orthophosphate.[26] For example, X-ray diffraction (XRD) and X-ray absorption near edge structure (XANES) analyses of dairy manure showed 57% dicalcium phosphate ($CaHPO_4$) and 43% struvite ($MgNH_4PO_4$).[26] High Ca:P ratio can transform dicalcium phosphate to hydroxyapatite.[27] Anaerobic digestion stabilized P in dairy manure to 78.2% struvite and 21.8% hydroxyapatite.[26] Whitlockite ($(Ca, Mg)_3(PO_4)_2$) has been observed in ≥500 °C manure biochars.[28] During extraction, P species are likely to dissolve together with the bound elements: Mg (struvite, whitlockite),[29] Ca (Ca orthophosphate),[30] Al, and Fe (hydr)-oxides.[31] Calcium phosphate and P species bound to small Fe (hydr)oxide particles[32] are sensitive to acid dissolution in the presence of oxalate ligand.[33] In contrast, P species bound to organic carbon are expected to require stronger ligand, EDTA, at higher pH to minimize the competition with protons.[34] Organic carbon fraction of biochar could directly bind orthophosphate and pyrophosphate through H-bonding interactions.[35] Alternatively, cations (especially Al^{3+} and Fe^{3+}) may facilitate the formation of organic carbon-bridging metal-P complexes.[36]

To investigate the influence of bound elements, Table 2 presents total P, Ca, K, Na, Mg, Al, Fe, Mn, and Zn concentrations determined in NaOH−EDTA and oxalate extracts. In NaOH−EDTA extracts (Table 2, left), the following increasing strength of Pearson's correlation (p < 0.0005, n = 12 without the outlier, sewage) was observable with P concentration: Zn (r = 0.89) < Mn (r = 0.90) < Mg (r = 0.98). In oxalate, the strength of correlation (p < 0.0005, n = 11 after removing the outliers sewage and FL700; note Al, Fe, Mn, and Zn are below detection limit for PS25-PS700) increased from Al (r = 0.87), Zn (r = 0.89), Fe (r = 0.92), Mn (r = 0.99), to Mg (r = 1.0). In conclusion, Mg orthophosphate,[26] struvite, and whitlockite are the likely sources of dissolved P in both NaOH−EDTA and oxalate extracts. Acidic pH (in the presence of oxalate) was required to dissolve Al- and Fe-bound P. However, Mg, Al, and Fe could facilitate (bridge) P binding on organic carbon.[36] Colloidal P species (associated with Al, Fe, and DOC)[6] are likely to form in oxalate extracts obtained by acidifying NaOH−EDTA. Oxalate is able to release P from Ca phosphate by forming stable calcium oxalate phases (K_{SO} = $10^{-8.75}$).[34] As a result, Ca concentrations in the oxalate extract (Table 2) are below detection limit for all biochars except sewage, SW25, SW350, and SW700. Low (e.g., citrate) and high (e.g., PAM) molecular weight dissolved ligands[7] in sewage and swine biochars could inhibit the growth, and change the morphology of calcium oxalate precipitates.[37]

Dissolved Phosphorus Speciation of Sequential Extracts. To understand the individual P species contributing to extractable P concentrations in Table 1, NaOH−EDTA and oxalate sequential extracts were analyzed by solution-phase ^{31}P

DOI: 10.1021/acssuschemeng.5b00336
ACS Sustainable Chem. Eng. 2015, 3, 1642−1649

Table 2. Dissolved P, Ca, K, Na, Mg, Al, Fe, Mn, and Zn Concentrations (mg kg^{-1}) in Sequential Extracts: Basic EDTA Followed by Acidic Oxalate[a]

	NaOH–EDTA (mg kg^{-1})										oxalate (mg kg^{-1})									
biochar	P	Ca	Ca:P	K	Na[b]	Mg	Al	Fe	Mn	Zn	P	Ca	K	Na	Mg	Al	Fe	Mn	Zn
corn	1302	10826	8.3	9424	91485	1797	0	17	86	19	405	0	1842	13468	329	91	184	25	0
sewage	16718	15725	0.9	8455	132344	6681	1086	3598	48	390	7719	2096	864	2779	2439	1146	13540	0	142
FP	120	413	3.5	4405	107916	235	0	116	42	0	27	0	592	5890	235	0	352	0	0
FL25	6995	17712	2.5	25096	148122	4389	0	84	143	258	514	0	1572	7675	226	24	119	0	0
FL350	11853	23121	2.0	31208	100865	5501	0	44	217	314	587	0	3589	7669	559	72	337	0	34
FL700	5349	13180	2.5	40177	107039	2787	35	8	62	169	N/A								
SW25	20438	22756	1.1	13686	133974	9505	0	359	917	2424	3207	13313	1422	10134	2037	119	778	102	220
SW350	24120	17076	0.7	13521	112830	9880	0	41	863	1382	5160	2223	1608	4930	3565	138	975	161	401
SW700	22886	5352	0.2	23208	114558	13667	0	0	413	1443	8634	1086	1466	2245	5311	162	1084	303	292
PS25	141	1566	11.1	2321	112402	311	0	0	0	0	21	0	37	1043	48	0	0	0	0
PS300	224	1718	7.7	2172	127486	287	0	0	0	0	17	0	125	2361	30	0	0	0	0
PS500	81	1597	19.8	1523	111894	41	0	0	0	0	12	0	25	226	7	0	0	0	0
PS700	50	1940	38.5	2195	112974	99	0	0	0	0	18	0	65	485	15	0	0	0	0

[a]Underlined values indicate an increase in the oxalate extract. [b]Set by 0.25 M NaOH in the NaOH–EDTA extraction fluid.

NMR. Of various extractants, NaOH–EDTA is reported to give diverse P species and highest diester:monoester ratio.[38] However, because EDTA strongly complexes paramagnetic ions,[34] peak broadening results from high Mn (and Fe to a lesser extent) concentration.[38] In addition, high pH of NaOH–EDTA can hydrolyze orthophosphate diester, e.g., phospholipids to monoester, and EDTA-complexed Mn and Fe cause poor separation of orthophosphate peak from monoester peaks.[38]

Figure 1 presents solution-phase ^{31}P NMR spectra of NaOH–EDTA (left) and oxalate (right) sequential extracts

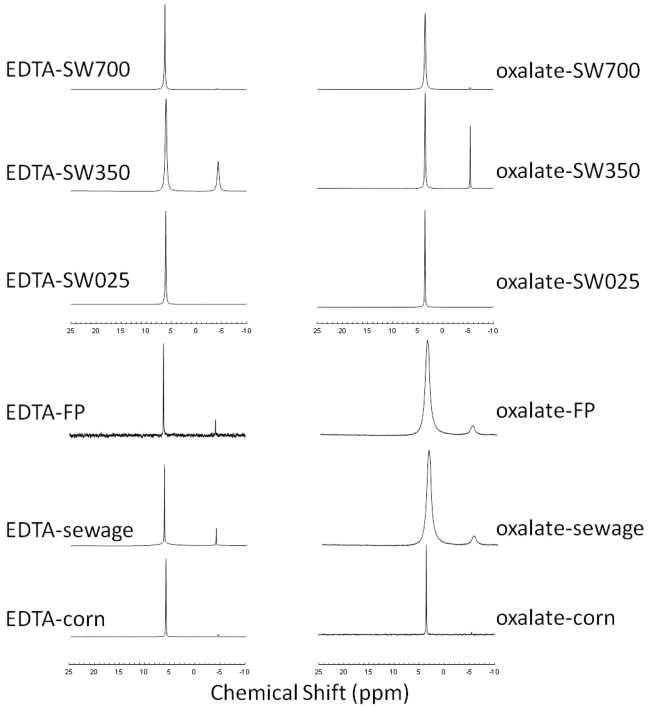

Figure 1. Solution-phase ^{31}P NMR spectra of NaOH–EDTA (250 mM NaOH+5 mM EDTA for 16 h, left) and oxalate (200 mM oxalate at pH 3.5 for 4 h, right) sequential extracts of swine manure feedstock (SW25) and 350 (SW350), 700 °C (SW700) slow pyrolysis biochars, sawdust-derived fast pyrolysis biochar (FP), and flash carbonization charcoals prepared from sewage sludge (sewage) and corn stover (corn). Chemical shifts (ppm) were determined with respect to 85% H_3PO_4 solution (0 ppm).

of swine manure slow pyrolysis biochars, sawdust-derived fast pyrolysis biochar, and flash carbonization charcoals prepared from sewage sludge and corn stover. Spectra for other slow pyrolysis biochars are provided in Figure S1 of the Supporting Information. Spectra for NaOH–EDTA extracts (Figure 1, left) are dominated by inorganic orthophosphate (PO_4^{3-} at 6.2 ppm) and pyrophosphate ($P_2O_7^{4-}$ at −4.1 ppm) peaks. Pyrophosphate is produced by heating orthophosphate above 300 °C.[39] Monoesters including phytate appear at 3–7 ppm, and diesters including DNA appear between −1.5 and +2.1 ppm.[18] Minor (<1%) polyphosphate (−20 ppm)[38] peaks were observable in NaOH–EDTA extract of SW350, and oxalate extracts of SW350 and FL25.

Compared to NaOH–EDTA (Figure 1, left), peaks were shifted toward lower ppm values in oxalate, because of lower pH. In addition, orthophosphate (3.57–3.79 ppm) and pyrophosphate (−5.2 to −5.4 ppm) peaks were broadened in oxalate extracts of FP and sewage, compared to NaOH–EDTA

DOI: 10.1021/acssuschemeng.5b00336
ACS Sustainable Chem. Eng. 2015, 3, 1642–1649

Table 3. Phosphorus Speciation of NaOH−EDTA (250 mM NaOH+5 mM EDTA for 16 h) and Oxalate (250 mM NaOH+5 mM EDTA for 16 h) Sequential Extracts Determined by ^{31}P NMR[a]

NaOH−EDTA extracts						
	inorganic P in mg kg^{-1} (% total)			organic P in mg kg^{-1} (% total)		
biochar	orthophosphate	pyrophosphate	total	monoesters[b]	diesters[c]	total
corn	1264 (97%)	38 (3%)	1302 (100%)	0	0	0
sewage	14345 (86%)	2373 (14%)	16718 (100%)	0	0	0
FP	106 (89%)	14 (11%)	120 (100%)	0	0	0
FL25	6264 (90%)	117 (2%)	6382 (91%)	421 (6%)	192 (3%)	613 (9%)
FL350	10770 (91%)	1065 (9%)	11835 (100%)	18 (0%)	0	18 (0%)
FL700	5342 (100%)	7 (0%)	5349 (100%)	0	0	0
SW25	20191 (99%)	64 (0%)	20255 (99%)	75 (0%)	108 (1%)	183 (1%)
SW350[d]	17736 (74%)	6352 (26%)	24088 (100%)	0	32 (0%)	32 (0%)
SW700	22588 (99%)	298 (1%)	22886 (100%)	0	0	0
PS25	36 (26%)	0	36 (26%)	105 (74%)	0	105 (74%)
PS300	107 (48%)	117 (52%)	224 (100%)	0	0	0
PS500	51 (62%)	30 (38%)	81 (100%)	0	0	0
PS700	39 (77%)	11 (23%)	50 (100%)	0	0	0

oxalate extracts			
biochar	inorganic P in mg kg^{-1} (% total)		
	orthophosphate	pyrophosphate	total
corn	398 (98%)	7 (2%)	405 (100%)
sewage	7103 (92%)	616 (8%)	7719 (100%)
FP	25 (93%)	2 (7%)	27 (100%)
FL25[e]	508 (99%)	6 (1%)	514 (100%)
FL350	530 (90%)	57 (10%)	587 (100%)
FL700	100%	0	100%
SW25	3202 (100%)	5 (0%)	3207 (100%)
SW350[f]	4145 (80%)	1015 (20%)	5160 (100%)
SW700	8553 (99%)	81 (1%)	8634 (100%)

[a]Values in parentheses represent % contribution of each P species to the total P in each extract (Table 1 provides absolute values in mg kg^{-1}). The ^{31}P NMR signals were below detection limit for the oxalate extracts of pecan shell biochars. [b]Including phytate (3 to 7 ppm). [c]Including DNA (−1.5 to +2.1 ppm). [d]Minor polyphosphate peaks in NaOH−EDTA extract of SW350. [e]Minor polyphosphate peaks in oxalate extracts of FL25 (0.7%). [f]Minor polyphosphate peaks in oxalate extracts of SW350 (0.2%).

(Figure 1). Table 2 presents concentrations of paramagnetic ions (Fe and Mn) in NaOH−EDTA and oxalate extracts. As reported previously,[38] NaOH−EDTA extracted higher amounts of Mn than Fe, except for sewage sludge flash carbonization charcoal containing over 20 wt $\%_{dry}$ Fe_2O_3.[40] On the other hand, Fe concentration in oxalate was higher than the preceding NaOH−EDTA step (underlined values in Table 2). Although low Fe and Mn concentrations are useful for increasing the signal relaxation rates and lowering the delay times between pulses, high concentration results in fast relaxation that causes line broadening.[41] Cation exchange resins and additives (e.g., Chelex-100, 8-hydroxyquinoline, Na_2S) have been utilized for the removal of paramagnetic ions prior to ^{31}P NMR analysis.[41] Line broadening and decreased peak resolution are also caused by high salt and organic carbon concentrations leading to the formation of fine particulates in the NMR samples.[41] Colloidal precipitates in acidic oxalate extracts could increase the viscosity of the NMR sample to cause line broadening.

Table 3 presents ^{31}P NMR peak integration results for inorganic (orthophosphate, pyrophosphate, polyphosphate, and total inorganic P) and organic P species (monoesters including phytate, diesters including DNA, and total organic P) in NaOH−EDTA and oxalate sequential extracts. The monoester region was integrated as a whole, because of well-documented signal overlap.[42] Absolute values in Table 3 are given in mg kg^{-1} biochar. These values were calculated by multiplying the fraction of integrated area (with respect to the total area) by the total P concentrations in NaOH−EDTA and oxalate (Table 1). In Table 3, values in parentheses represent % contribution of each P species to the NaOH−EDTA and oxalate-extractable P in Table 1. In NaOH−EDTA, feedlot and swine manures and biochars were dominated by inorganic orthophosphate, and the contribution of monoesters was less than 6%. This is a striking contrast to broiler litter manure containing 58% phytate.[3] Upon pyrolysis at 350 °C, organic P species in both swine and feedlot manures nearly disappeared (Table 3), and inorganic orthophosphate continued to dominate up to 700 °C, except for the significant contribution of pyrophosphate in SW350 (26%). In contrast, pecan shell feedstock was primarily (74%) phytate with lower orthophosphate fraction (26%) than manures. At 300 °C, phytate disappeared, and pyrophosphate (52%) and orthophosphate (48%) became equally dominant. At 500 °C and above, orthophosphate began to outweigh pyrophosphate, resulting in 77% orthophosphate at 700 °C (Table 3). These temperature trends agree with our previous report on plant (cottonseed hull)-derived biochars containing 1 order of magnitude higher NaOH−EDTA-extractable P than pecan shell biochars.[3] Flash carbonization (corn and sewage) and fast pyrolysis (FP) biochars were dominated by orthophosphate, except for significant (14%) contribution of pyrophosphate on sewage (Table 3). High contribution of

DOI: 10.1021/acssuschemeng.5b00336
ACS Sustainable Chem. Eng. 2015, 3, 1642−1649

pyrophosphate in SW350 (26%), sewage (14%), and 300−700 °C pecan shell biochars (23−52%) suggest complexation by organic carbon fraction of biochar.[3] Orthophosphate concentrations in Table 3 strongly ($p < 0.0005$, $n = 13$) correlated with Mg ($r = 0.98$) and Zn ($r = 0.88$) concentrations, much like the total P concentrations in NaOH−EDTA extract (Table 1). In conclusion, Mg orthophosphate (and struvite)[26] likely exist in all biochars investigated in this study. For pyrophosphate, no correlation was observed with elements listed in Table 2 or VM and other bulk parameters in Table 1.

In the subsequent acidic oxalate extracts, a similar distribution of inorganic P species was observed as the preceding NaOH−EDTA step (Table 3). In particular, pyrophosphate concentrations in EDTA and oxalate extracts showed a similar trend for different biochars ($r = 0.97$, $p < 0.0005$, $n = 8$, without FL700). Values were below the detection limit for pecan shell biochars, because of orders of magnitude lower oxalate-extractable P than other biochars (Table 1). In conclusion, majority of organic P species was removed (or underwent acid hydrolysis during the oxalate extraction) from all biochars by a strong ligand (EDTA) at high pH. In the subsequent step, remaining orthophosphate and pyrophosphate were released from calcium phosphate (by forming Ca oxalate) and other phases sensitive to acid dissolution, e.g., P bound on Fe and Al (hydr)oxide.

Solid-State ^{13}C CPMAS NMR Analysis of Bulk Aromaticity. Persistence of pyrophosphate in sewage, SW350, and PS300-PS700 (but not in other biochars) suggests the involvement of organic carbon (instead of ash) fraction of biochar.[3] Organic carbon fraction of biochar could (i) directly bind pyrophosphate by H-bonding,[35] or (iii) utilize bridging cations to from organic carbon-bridging metal-P complexes.[36] To visualize the surface functionalities that could bind pyrophosphate, Figure 2 presents solid-state ^{13}C CPMAS NMR spectra of slow/fast pyrolysis and flash carbonization charcoals. Spinning sidebands (SSBs marked as asterisks in Figure 2) appear in both sides of a peak at equal intensity. The SSBs are artifacts caused when magic angle spinning is less than the chemical shift anisotropy for a given resonance.[43] For aromatic C (−C═C− at 110−160 ppm) of SW700 and FL700, SSBs are visible in both lower and higher sides of the magnetic fields, each 60−70 ppm apart from the peak. In FP, sewage, and corn (Figure 2, left), SSBs are only visible at the lower magnetic field; "hidden" SSBs at higher magnetic fields could lead to the misinterpretation of the peak integration results. Therefore, solid-state ^{13}C CPMAS NMR spectra in Figure 2 were interpreted qualitatively for the following chemical shift regions (in ppm): aliphatic C (0−45), O/N alkyl C (45−110), aromatic C (110−160), and carbonyl C (160−190).[22]

In Figure 2, aromatic (−C═C− peak centered at 130 ppm) nature of fast pyrolysis biochar (FP) is in agreement with its high fixed C content (Table 1) that is influenced by the length of time FP was exposed to the heated fluidized bed. The spectra for 700 °C manure biochars (both swine and feedlot) were dominated by the aromatic peak (-C═C−) at 110−160 ppm, in agreement with the literature reports for high HTT slow pyrolysis biochars.[43] Compared to 350 °C biochars produced from feedlot (Figure 2) and broiler litter,[7] swine solid 350 °C biochar contained a sharp methylene (CH_2) peak at 35 ppm indicative of long-chain alkyl groups. This is in agreement with the FTIR spectrum of unpyrolyzed swine solids having unusually sharp C—H stretching band that persisted after pyrolysis at 350 °C.[14] Uniquely aliphatic nature of swine solids

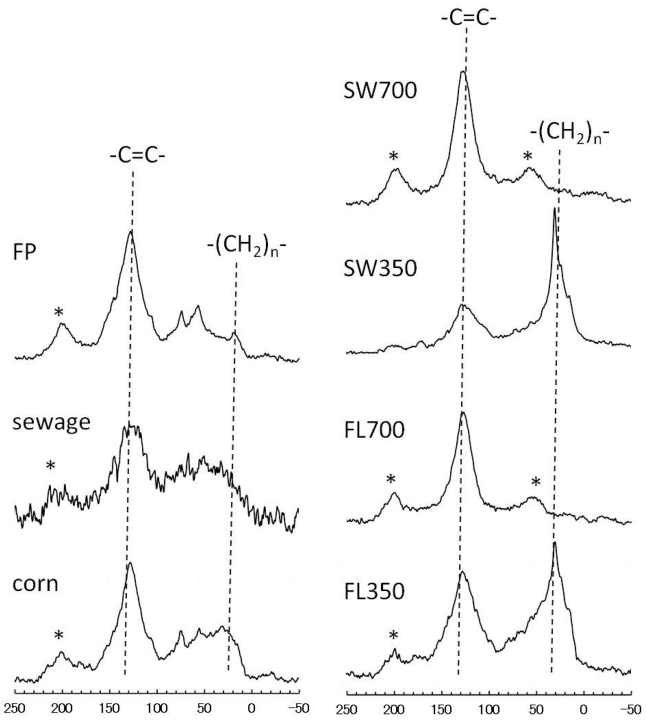

Figure 2. Solid-state ^{13}C CPMAS NMR spectra of sawdust-derived fast pyrolysis biochar (FP); flash carbonization charcoals prepared from sewage sludge (sewage) and corn stover (corn); 350 and 700 °C slow pyrolysis biochars prepared from swine (SW) and feedlot (FL) manures.

(compared to feedlot, poultry litter, turkey litter, and dairy manures) had been attributed to the stability of PAM toward thermochemical conversion.[14] In addition, PAM could stabilize P in swine manure during pyrolysis,[14] and serve as the growth media to form crystalline hydroxyapatite.[44,45] Persistence of pyrophosphate in biochars having low aromaticity (SW350 and sewage in Figure 2) suggests binding by the surface functional groups enriched in partially carbonized biochars. Ligand exchange and surface precipitation are the stabilization mechanisms of both organic[46] and inorganic[47] P species in soils. Carboxyl and hydroxyl are likely functional groups of biochar[48] to complex bridging cations such as Al^{3+}, Fe^{3+}, Mg^{2+}, and Ca^{2+} to form stable six-membered ring complexes with pyrophosphate.[34] Alternatively, depending on solution pH, surface functional groups of biochar could directly bind pyrophosphate through H-bonding interactions.[35]

■ ASSOCIATED CONTENT

Supporting Information

Solution-phase ^{31}P NMR spectra of pecan shell and feedlot slow pyrolysis biochars. The Supporting Information is available free of charge on the ACS Publications website at DOI: 10.1021/acssuschemeng.5b00336.

■ AUTHOR INFORMATION

Corresponding Author

*M. Uchimiya. Fax: (504) 286-4367. Phone: (504) 286-4356. E-mail: sophie.uchimiya@ars.usda.gov.

Notes

The authors declare no competing financial interest.

DOI: 10.1021/acssuschemeng.5b00336
ACS Sustainable Chem. Eng. 2015, 3, 1642−1649

■ ACKNOWLEDGMENTS

The authors acknowledge Dr. Keri Cantrell for providing manure biochar samples. Mention of trade names or commercial products in this publication is solely for the purpose of providing specific information and does not imply recommendation or endorsement by the U.S. Department of Agriculture. USDA is an equal opportunity provider and employer.

■ REFERENCES

(1) van Straaten, P. *Rocks for Crops: Agrominerals of sub-Saharan Africa*; International Centre for Research in Agroforestry: Nairobi, Kenya, 2002; p 338.
(2) Gilbert, N. The disappearing nutrient. *Nature* **2009**, *461*, 716−718.
(3) Uchimiya, M.; Hiradate, S. Pyrolysis temperature-dependent changes in dissolved phosphorus speciation of plant and manure biochars. *J. Agric. Food Chem.* **2014**, *62*, 1802−1809.
(4) Basile-Doelsch, I.; Balesdent, J.; Rose, J. Are interactions between organic compounds and nanoscale weathering minerals the key drivers of carbon storage in soils? *Environ. Sci. Technol.* **2015**, *49*, 3997−3998.
(5) Hens, M.; Merckx, R. Functional characterization of colloidal phosphorus species in the soil solution of sandy soils. *Environ. Sci. Technol.* **2001**, *35*, 493−500.
(6) Montalvo, D.; Degryse, F.; McLaughlin, M. J. Natural colloidal P and its contribution to plant P uptake. *Environ. Sci. Technol.* **2015**, *49*, 3427−3434.
(7) Uchimiya, M.; Hiradate, S.; Antal, M. J. Influence of carbonization methods on the aromaticity of pyrogenic dissolved organic carbon. *Energy Fuels* **2015**, *29*, 2503−2513.
(8) Antal, M. J., Jr.; Varhegyi, G. Impact of systematic errors on the determination of cellulose pyrolysis kinetics. *Energy Fuels* **1997**, *11*, 1309−1310.
(9) Narayan, R.; Antal, M. J. Thermal lag, fusion, and the compensation effect during biomass pyrolysis. *Ind. Eng. Chem. Res.* **1996**, *35*, 1711−1721.
(10) Lede, J. Biomass pyrolysis: Comments on some sources of confusions in the definitions of temperatures and heating rates. *Energies* **2010**, *3*, 886−898.
(11) Antal, M. J.; Gronli, M. The art, science, and technology of charcoal production. *Ind. Eng. Chem. Res.* **2003**, *42*, 1619−1640.
(12) Branca, C.; Di Blasi, C. Multistep mechanism for the devolatilization of biomass fast pyrolysis oils. *Ind. Eng. Chem. Res.* **2006**, *45*, 5891−5899.
(13) Uchimiya, M. Influence of pH, ionic strength, and multidentate ligand on the interaction of Cd^{II} with biochars. *ACS Sustainable Chem. Eng.* **2014**, *2*, 2019−2027.
(14) Cantrell, K. B.; Hunt, P. G.; Uchimiya, M.; Novak, J. M.; Ro, K. S. Impact of pyrolysis temperature and manure source on physicochemical characteristics of biochar. *Bioresour. Technol.* **2012**, *107*, 419−428.
(15) Mejia Likosova, E.; Keller, J.; Rozendal, R. A.; Poussade, Y.; Freguia, S. Understanding colloidal FeSx formation from iron phosphate precipitation sludge for optimal phosphorus recovery. *J. Colloid Interface Sci.* **2013**, *403*, 16−21.
(16) Antal, M. J., Jr.; Mochidzuki, K.; Paredes, L. S. Flash carbonization of biomass. *Ind. Eng. Chem. Res.* **2003**, *42*, 3690−3699.
(17) Brewer, C. E.; Schmidt-Rohr, K.; Satrio, J. A.; Brown, R. C. Characterization of biochar from fast pyrolysis and gasification systems. *Environ. Prog. Sustainable Energy* **2009**, *28*, 386−396.
(18) Turner, B. L.; Mahieu, N.; Condron, L. M. Phosphorus-31 nuclear magnetic resonance spectral assignments of phosphorus compounds in soil NaOH-EDTA extracts. *Soil Sci. Soc. Am. J.* **2003**, *67*, 497−510.
(19) U.S. EPA. *Method 200.7 Trace Elements in Water, Solids, and Biosolids by Inductively Coupled Plasma-Mass Spectrometry*, Revision 5.0; EPA-821-R-01−010; United States Environmental Protection Agency, Office of Research and Development: Cincinnati, OH, 2001.
(20) Uchimiya, M.; Orlov, A.; Ramakrishnan, G.; Sistani, K. In situ and ex situ spectroscopic monitoring of biochar's surface functional groups. *J. Anal. Appl. Pyrol.* **2013**, *102*, 53−59.
(21) Turner, B. L.; Condron, L. M.; Richardson, S. J.; Peltzer, D. A.; Allison, V. J. Soil organic phosphorus transformations during pedogenesis. *Ecosystems* **2007**, *10*, 1166−1181.
(22) Ono, K.; Hiradate, S.; Morita, S.; Hirai, K. Fate of organic carbon during decomposition of different litter types in Japan. *Biogeochemistry* **2013**, *112*, 7−21.
(23) Zhao, L.; Cao, X.; Wang, Q.; Yang, F.; Xu, S. Mineral constituents profile of biochar derived from diversified waste biomasses: Implications for agricultural applications. *J. Environ. Qual.* **2013**, *42*, 545−552.
(24) Enders, A.; Lehmann, J. Comparison of wet-digestion and dry-ashing methods for total elemental analysis of biochar. *Commun. Soil Sci. Plan.* **2012**, *43*, 1042−1052.
(25) Knicker, H. How does fire affect the nature and stability of soil organic nitrogen and carbon? A review. *Biogeochemistry* **2007**, *85*, 91−118.
(26) Güngör, K.; Jürgensen, A.; Karthikeyan, K. G. Determination of phosphorus speciation in dairy manure using XRD and XANES spectroscopy. *J. Environ. Qual.* **2007**, *36*, 1856−1863.
(27) Toor, G. S.; Peak, J. D.; Sims, J. T. Phosphorus speciation in broiler litter and turkey manure produced from modified diets. *J. Environ. Qual.* **2005**, *34*, 687−697.
(28) Cao, X. D.; Harris, W. Properties of dairy-manure-derived biochar pertinent to its potential use in remediation. *Bioresour. Technol.* **2010**, *101*, 5222−5228.
(29) Hunger, S.; Sims, J. T.; Sparks, D. L. Evidence for struvite in poultry litter: Effect of storage and drying. *J. Environ. Qual.* **2008**, *37*, 1617−1625.
(30) Seiter, J. M.; Staats-Borda, K. E.; Ginder-Vogel, M.; Sparks, D. L. XANES spectroscopic analysis of phosphorus speciation in alum-amended poultry litter. *J. Environ. Qual.* **2008**, *37*, 477−485.
(31) Darke, A. K.; Walbridge, M. R. Al and Fe biogeochemistry in a floodplain forest: Implications for P retention. *Biogeochemistry* **2000**, *51*, 1−32.
(32) Iyengar, S. S.; Zelazny, L. W.; Martens, D. C. Effect of photolytic oxalate treatment on soil hydroxy-interlayered vermiculites. *Clays Clay Miner.* **1981**, *29*, 429−434.
(33) Ohno, T.; Hiradate, S.; He, Z. Phosphorus solubility of agricultural soils: A surface charge and phosphorus-31 NMR speciation study. *Soil Sci. Soc. Am. J.* **2011**, *75*, 1704−1711.
(34) Martell, A. E.; Smith, R. M.; Motekaitis, R. J. *Critically Selected Stability Constants of Metal Complexes Database*; U.S. Department of Commerce, National Institute of Standards and Technology: Gaithersburg, MD, 2004.
(35) Chen, Z.; Xiao, X.; Chen, B.; Zhu, L. Quantification of chemical states, dissociation constants and contents of oxygen-containing groups on the surface of biochars produced at different temperatures. *Environ. Sci. Technol.* **2015**, *49*, 309−317.
(36) Gerke, J. Humic (organic matter)-Al(Fe)-phosphate complexes: An underestimated phosphate form in soils and source of plant-available phosphate. *Soil Sci.* **2010**, *175*, 417−425.
(37) Qiu, S. R.; Wierzbicki, A.; Orme, C. A.; Cody, A. M.; Hoyer, J. R.; Nancollas, G. H.; Zepeda, S.; De Yoreo, J. J. Molecular modulation of calcium oxalate crystallization by osteopontin and citrate. *Proc. Natl. Acad. Sci. U. S. A.* **2004**, *101*, 1811−1815.
(38) Cade-Menun, B. J.; Preston, C. M. A comparison of soil extraction procedures for ^{31}P NMR spectroscopy. *Soil Sci.* **1996**, *161*, 770−785.
(39) Miller, S. L.; Parris, M. Synthesis of pyrophosphate under primitive earth conditions. *Nature* **1964**, *204*, 1248−1250.
(40) Van Wesenbeeck, S.; Prins, W.; Ronsse, F.; Antal, M. J. Sewage sludge carbonization for biochar applications. Fate of heavy metals. *Energy Fuels* **2014**, *28*, 5318−5326.
(41) Cade-Menun, B.; Liu, C. W. Solution phosphorus-31 nuclear magnetic resonance spectroscopy of soils from 2005 to 2013: A review

DOI: 10.1021/acssuschemeng.5b00336
ACS Sustainable Chem. Eng. 2015, 3, 1642−1649

of sample preparation and experimental parameters. *Soil Sci. Soc. Am. J.* **2014**, *78*, 19−37.
(42) Vestergren, J.; Vincent, A. G.; Jansson, M.; Persson, P.; Ilstedt, U.; Gröbner, G.; Giesler, R.; Schleucher, J. High-resolution characterization of organic phosphorus in soil extracts using 2D ^{1}H-^{31}P NMR correlation spectroscopy. *Environ. Sci. Technol.* **2012**, *46*, 3950−3956.
(43) McBeath, A. V.; Smernik, R. J.; Krull, E. S.; Lehmann, J. The influence of feedstock and production temperature on biochar carbon chemistry: A solid-state ^{13}C NMR study. *Biomass Bioenergy* **2014**, *60*, 121−129.
(44) Yokoi, T.; Kawashita, M.; Kikuta, K.; Ohtsuki, C. Crystallization of calcium phosphate in polyacrylamide hydrogels containing phosphate ions. *J. Cryst. Growth* **2010**, *312*, 2376−2382.
(45) Yokoi, T.; Kawashita, M.; Kikuta, K.; Ohtsuki, C. Biomimetic mineralization of calcium phosphate crystals in polyacrylamide hydrogel: Effect of concentrations of calcium and phosphate ions on crystalline phases and morphology. *Mater. Sci. Eng., C* **2010**, *30*, 154−159.
(46) Yan, Y.; Li, W.; Yang, J.; Zheng, A.; Liu, F.; Feng, X.; Sparks, D. L. Mechanism of myo-inositol hexakisphosphate sorption on amorphous aluminum hydroxide: Spectroscopic evidence for rapid surface precipitation. *Environ. Sci. Technol.* **2014**, *48*, 6735−6742.
(47) Wang, L.; Putnis, C. V.; Ruiz-Agudo, E.; Hövelmann, J.; Putnis, A. In situ imaging of interfacial precipitation of phosphate on goethite. *Environ. Sci. Technol.* **2015**, *49*, 4184−4192.
(48) Keiluweit, M.; Nico, P. S.; Johnson, M. G.; Kleber, M. Dynamic molecular structure of plant biomass-derived black carbon (biochar). *Environ. Sci. Technol.* **2010**, *44*, 1247−1253.
(49) Uchimiya, M.; Ohno, T.; He, Z. Pyrolysis temperature-dependent release of dissolved organic carbon from plant, manure, and biorefinery wastes. *J. Anal. Appl. Pyrol.* **2013**, *104*, 84−94.

DOI: 10.1021/acssuschemeng.5b00336
ACS Sustainable Chem. Eng. 2015, 3, 1642−1649